Y/NSP-305

National Security Program Office

MICROCHIP DEVICE FOR LIQUID PHASE ANALYSIS

Final Report

J. M. Ramsey
Oak Ridge National Laboratory

May 2000

May 2000 **Y/NSP-305**

National Security Program Office

MICROCHIP DEVICE FOR LIQUID PHASE ANALYSIS

Final Report

J. M. Ramsey
Oak Ridge National Laboratory

prepared by
NATIONAL SECURITY PROGRAM OFFICE
OAK RIDGE Y-12 PLANT
OAK RIDGE, TENNESSEE 37831-8206
managed by
LOCKHEED MARTIN ENERGY SYSTEMS, INC.
for the
DEPARTMENT OF ENERGY
under contract DE-AC05-84OR21400

CONTENTS

Page

1. SUMMARY

The lab-on-a-chip concept has enabled miniature instruments to be developed that allow the rapid execution and automation of fluidic operations such as valving, separation, dilution, mixing, and flow splitting upon the proper application of a motive (driving) force. The integration of these simple operations to perform complete, multiple-step chemical assays is rapidly becoming a reality.[1, 2] Such compact, monolithic devices potentially enjoy advantages in speed, cost, automation, reagent consumption, and waste generation compared to existing laboratory-scale instruments.

Initial reports of these microfluidic devices focused on combining various electrokinetically driven separation methods including microchip electrophoresis,[3-7] gel electrophoresis,[8-10] micellar electrokinetic chromatography (MEKC)[11, 12] and open channel electrochromatography (OCEC)[13] with fluidic valving to introduce sample plugs into the separation channel. Other operations have quickly been integrated with the separations and fluidic valving on these microchips. For example, integrated devices with mixers/diluters for precolumn[14-16] and postcolumn[17, 18] analyte derivitization, deoxyribonucleic acid (DNA) restriction digests,[15] enzyme assays,[19, 20] and polymerase chain reaction (PCR) amplification[21, 22] have been added to the basic design. Integrated mixers that can perform solvent programming for both MEKC[23] and OCEC[24] have also been demonstrated.

These examples are simple, yet powerful, demonstrations of the potential for lab-on-a-chip devices. In this report, three key areas for improved performance of these devices are described: on-chip calibration techniques, enhanced separative performance, and enhanced detection capabilities.

In brief, the calibration of analyses on microchips is shown using both internal standards and standard additions. The use of an internal standard allows the quantitation of an unknown concentration of analyte 1/10 to 10 times the concentration of the internal standard to an accuracy of 1%. The performance of standard additions to quantify an unknown concentration of analyte is not as good as that found with the use of an internal standard.

To enhance separative performance, the characteristics of samples injected onto the separation channel of a microfluidic device were determined through the manipulation of the electric field strengths during both the sample loading and dispensing steps. Three sample loading profiles for the constant volume valve (pinched injection) in conjunction with four dispensing schemes were investigated to assess their effect on injection and, therefore, separation performance. The sample confinement profiles for the sample-loading step consisted of a weakly pinched sample, a medium pinched sample, and a strongly pinched sample. Four dispensing schemes varied the electric field strengths in the sample and sample waste channels relative to the analysis channel to control the volume of the sample dispensed from the valve. The axial extent of the sample plug decreased as the electric field strengths in the sample and sample waste channels were raised relative to the analysis channel. In addition, a trade-off is shown to exist between sample plug length and sensitivity.

Detection limits were enhanced by combining sample stacking with sodium dodecyl sulfate (SDS) mediated sample sweeping to concentrate hydrophobic analytes on a microchip. Signal enhancements of 85- to 560-fold were achieved for injected samples in only 10 mm of stacking

distance. The intensity of the stacked, swept analyte zones was greater than that obtained by sweeping alone.

2. INTERNAL STANDARDS FOR CALIBRATION

2.1 INTRODUCTION

To ensure the proper quantitation of samples of interest, the ability to perform on-chip calibration is crucial. Compound identification using migration time or retention time data is more reliable if determined relative to a standard. The three most common methods used to calibrate assays are described briefly below. First, a set of standards may be run prior to an analysis to calibrate the instrumental response. Second, an internal standard may be included in the assay itself. The response of this internal standard with respect to both the instrument and the sample is determined prior to the analysis of the unknown sample. Third, the method of standard additions may be used. In this method, several assays of the sample are performed in which varying known amounts of the analyte are added to an unknown amount of the analyte in the sample. The instrumental responses to these known plus unknown concentrations are plotted against the known concentration of the analyte that has been added to the sample. The absolute value of the x-intercept of the regression line through these points gives the concentration of the analyte in the sample. For targeted analysis, the actual targets can be used as migration standards when using the method of standard addition. In this section of the report, we explore the use of internal standards and standard additions for quantification and identification of samples on microchips. The results are presented below.

2.2 EXPERIMENTS

2.2.1 Chemicals and Sample Derivatization. Arginine (Arg), alanine (Ala), aspartic acid (Asp), and rhodamine B (RhB) were all obtained from Sigma Chemical Company (St. Louis, Missouri). Tetramethylrhodamineisothiocyanate (TRITC) was obtained from Molecular Probes (Eugene, Oregon). Arginine, Ala, and Asp were derivatized with TRITC using the procedure provided by Molecular Probes.

2.2.2 Chip Designs and Operation. Microchips were fabricated on soda-lime glass (Gold Seal #3011; Gold Seal Products, Portsmouth, New Hampshire) using standard photolithographic patterning and wet chemical etching, as previously described.[13] A closed-channel network was formed by bonding another slide over the top of the etched structure. Access holes to the channels were ultrasonically drilled (Sonic-Mill, Albuquerque, New Mexico) into one of the slides prior to bonding. Small fluid reservoirs (140-μL capacity) were attached with Epo-tek 353ND epoxy (Epoxy Technologies, Inc., Billerica, Massachusetts) at points where the access holes were drilled.

Schematic diagrams of the chips used are shown in Fig. 2.1. The channel depths and the lengths of each arm are reported in Table 2.1. The chip structure shown in Fig. 2.1A was used for the internal standards experiments; the chip structure shown in Fig. 2.1B was used for the

standard addition experiments. The channels of the fork in the waste-1 channel of the chip in Fig. 2.1B were 250 µm long with a center-to-center spacing of 500 µm.

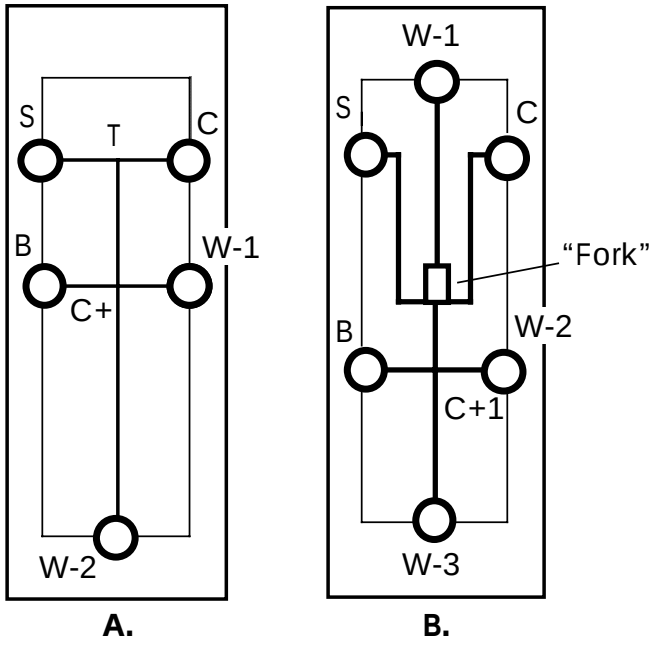

Fig. 2.1. Schematics of the two chip designs used to test the internal standard (A) and standard addition (B) calibration methods. The sample (S), calibrant (C), buffer (B),and waste(W) channels are labeled using one letter abbreviations. Tees(T) and crosses (C+) are also labeled in the same way.

Electrical contact with the chip was accomplished by inserting platinum electrodes into the reservoirs. The voltages applied to the chip were generated using four independent and remotely programmable high-voltage (0- to 4-kV) power supplies (Ultravolt 10A12-P4; Ultravolt, Ronkonkoma, New York). These supplies were controlled using multifunction input/output (I/O) cards (PCI-MIO16-XE50; National Instruments, Austin, Texas) in a Power Macintosh and software written with LabVIEW™ (National Instruments, Austin, Texas).

The running buffer used for the experiments was 10 mM sodium tetraborate/50 mM HEPES at pH 7.2. The analytes were injected using a gated sample introduction scheme.[17] Prior to each day's experiments, the chip was washed with 1 M NaOH and rinsed with distilled deionized water. The washes were carried out using vacuum aspiration. The vacuum was applied to each reservoir for 5 min.

Table 2.1. Channel depths, widths, and lengths used in the calibration experiments.

Chip	**2.1A**	**2.1B**
Depth (µm)	10	10.6
Width (µm)	50	42.4
Channel lengths (cm)		
S	.615	1.88
C	.685	1.90
B	.645	0.67
W-1	.665	1.43
W-2	2.35	0.73
W-3	NA	1.88
Mixing	2.6	0.5

2.2.3 Single Point Detection. Laser-induced fluorescence (LIF) detection of the analytes was performed using the 514-nm line of a Coherent Innova 90 Argon ion laser (Coherent, Inc., Palo Alto, California) as the excitation source at 15 mW. The laser beam was focused through a plano-convex lens (f = 12.5 cm; Esco Products, Inc., Oak Ridge, New Jersey) onto the channel. The fluorescence was collected using a 40X microscope objective (CD-240-M40X; Creative Devices, Neshanic Station, New Jersey) and was focused onto a 800-µm air pinhole (Melles Griot, Irvine, California).

The signal passing through the pinhole was then spectrally filtered using a 514-nm notch filter (Kaiser Optical Systems, Inc., Ann Arbor, Michigan) and a bandpass filter centered at 560 nm with a bandpass of 40 nm (560df40; Omega Optical, Brattleboro, Vermont) before being measured by a photomultiplier tube (PMT, 77348; Oriel Instruments, Inc., Stratford, Connecticut). The signal from the PMT was amplified using a SR570 low-noise current preamplifier (Stanford Research Systems, Inc., Sunnyvale, California) with a 10-ms filter. The signal from the amplifier was sampled at 100 Hz using a National Instruments PCI-MIO16-XE50 multifunction I/O card (National Instruments, Inc., Austin, Texas) in a Power Macintosh. The data acquisition was performed using the same LabVIEW program that was used for the high-voltage control.

2.2.4 Imaging. The microchips were imaged using a Nikon TE300 inverted microscope with an epifluorescence attachment and an 1152 x 770, charge-coupled device (CCD) camera (EEV 05-20; Princeton Instruments). The CCD camera was operated using an ST-138 controller (Princeton Instruments) that was interfaced to a Power Macintosh. The software package IPLab (Scanalytics, Inc., Fairfax, Virginia) was used to control the camera system and to acquire the images. A high-pressure mercury arc lamp was used for fluorescence excitation.

2.3 RESULTS AND DISCUSSION

2.3.1 Internal Standard. The experiments that examined the feasibility of using the internal standard method of calibration were carried out using the chip design in Fig. 2.1A. This is the simplest chip design that can be used to mix solutions from two different channels together at a tee (T) and, then, to inject the mixed sample at an injection cross (C+) into the separation channel. The chip was designed so that the contents of the sample and calibrant reservoirs would mix equally at the tee when equal potentials are applied to the two reservoirs. To quantitatively confirm the amount of mixing at the tee and to show that the amount of mixing could be precisely controlled using the potentials applied at the sample and calibrant reservoirs, the sample reservoir was filled with 0.1 mM RhB in running buffer while all of the other reservoirs where filled with running buffer only. Images of the mixing tee were then taken as the potentials on the sample, and calibrant reservoirs were varied in increments of 0.05 kV while keeping the sum of the voltages applied to the two reservoirs constant at 1.8 kV. Rhodamine B was then added to the calibrant reservoir and removed from the sample reservoir, and the procedure was reversed. Profiles across the mixing channel just above the injection valve were taken from these images, and the signals were integrated. This resulted in the signal vs voltage traces seen in Fig. 2.2. The relationship between the voltage applied and the concentration of RhB is linear from about 1% to 99% of the total signal. The correlation coefficients for the fitted lines were both 0.999+, and the slopes for the RhB concentration dispensed from the sample and calibration standard reservoirs were 1.78×10^7 and -1.77×10^7, respectively. The slopes are inversely related to one another as expected.

The same procedure was repeated on the single-point setup with the detection point 0.5 cm down the separation channel from the injection cross. This was done to demonstrate that the diffusional mixing was completed prior to the injection cross and that varying the potentials on the sample and calibrant reservoirs did not adversely affect the injection. A trace similar to that shown in Fig. 2.2 was obtained when the mixing channel length was 5 mm long. For a mixing channel length of 0.2 mm, the fluid streams from the sample and calibrant channels did not completely mix. This led to either a greater than expected or less than expected signal in the separation channel depending upon whether the RhB was added to the sample or calibrant reservoir.

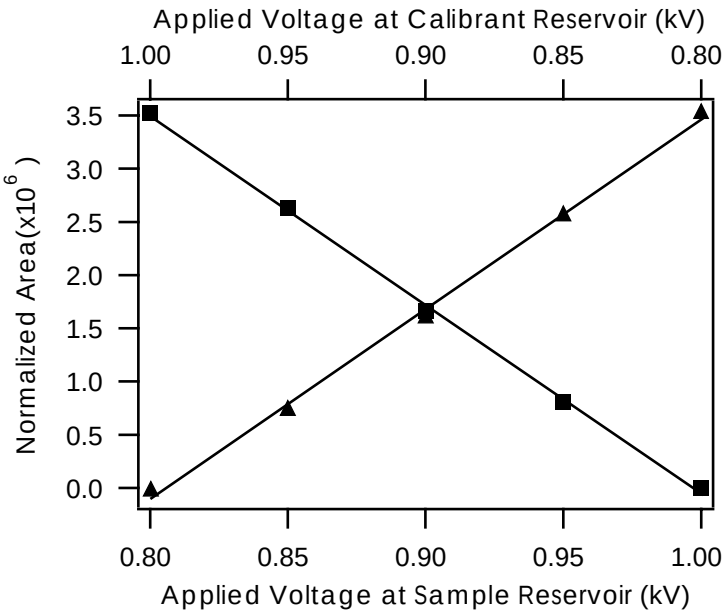

Fig. 2.2. Test of dispensing control from sample and calibration standard reservoirs (s sample reservoir, n sample reservoir).

To generate the actual calibration curve, TRITC derivatized Ala was used as the internal standard at a concentration of 10 µM. TRITC derivatized Ala and Asp were the analytes. Triplicate runs at each concentration were made. The analyte concentrations tested ranged from 1/10 to 10 times the concentration of the internal standard. The calibration curve generated for both TRITC-Ala and TRITC-Asp can be seen in Fig. 2.3. The correlation coefficients were both 0.9999 when plotted on a log-log scale, and the error bars are smaller than the symbols used to plot the data points. The slopes of the calibration curves are both near unity, with TRITC-Ala at 1.08 and TRITC-Asp at 1.06. The relative standard error for the determining the sample concentration values in a range from one order of magnitude higher and lower than the concentration of the internal standard was less than or equal to 1.0% for both the TRITC-Ala and the TRITC-Asp.

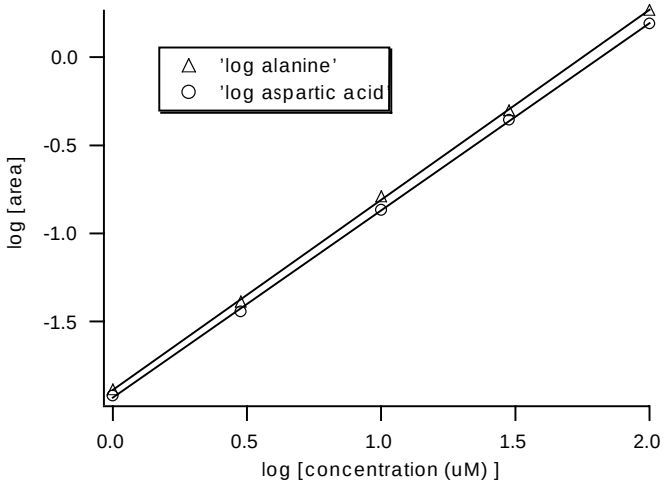

Fig. 2.3. Calibration curve generated using internal standard.

2.3.2 Standard Additions. To demonstrate the feasibility of performing sample calibration using standard additions, a chip design more complicated than that used for internal standards was needed (Fig. 2.1a). The added complexity is necessary because 100% flow from the analyte reservoir is required with the standard addition method of calibration. It is difficult with the previous internal standard chip design (Fig. 2.1a) to get 100% flow from either the analyte or calibration reservoirs without having the flow cross into the other channel and cause some cross-contamination between the two reservoirs. This chip design is unique in that it uses a "forked" waste-1 channel to ensure that the sample and calibrant cannot cross contaminate each other when 100% flow into the mixing channel is required from either the calibrant or sample channel. With this design, when 100% flow from one reservoir into the mixing channel is required, a small positive flow from the other reservoir to waste-1 through the fork of the waste-1 channel closest to that reservoir can also be realized.

When using the chip structure shown in Fig. 2.1B, therefore, the sample or calibration standards can be individually injected onto the separation channel, or they can be combined in any ratio desired by the operator. Simulation software for electronic circuit design was used to verify that the chip would work properly upon fabrication (Fig. 2.4). The resistor values in the circuit model are proportional to the channel dimensions. One critical goal in this design process was to keep the field strength in the separation channel constant for the analysis of the sample, the calibrant, or a combination of both. By keeping the separation field strength constant, analyte migration times and instrumental responses to the analytes coming out of the sample and calibration reservoirs will be the same. The result of a typical simulation where the separation channel field strength remains constant, independent of whether the sample or calibrant is used, is shown in Table 2.2. The mixing at the cross (C+1) was quantitated using the same method as was used for the tee on the internal standard chip. The results were the same.

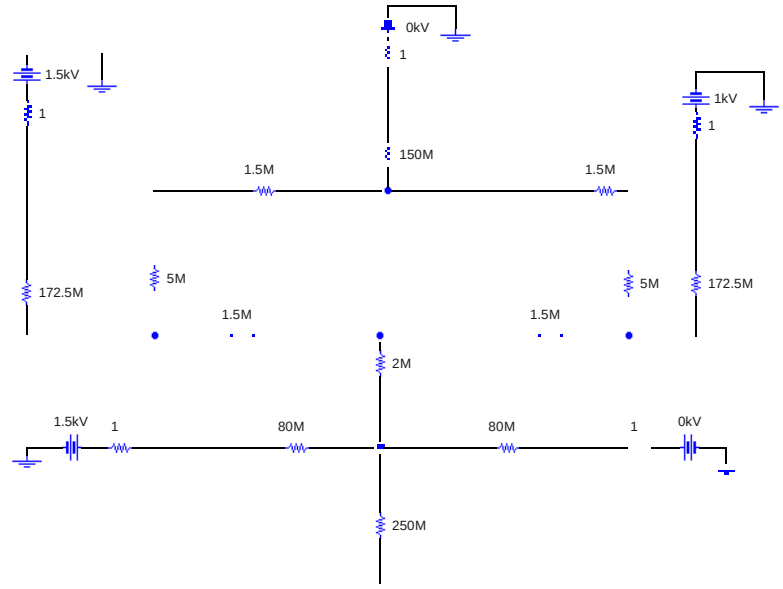

Fig. 2.4. Circuit model of chip.

Table 2.2. Results from the electronic circuit model of the chip.[a]

	Analysis conditions for respective sample		
Channels	Sample (V/cm)	Calibrant (V/cm)	Both (V/cm)
Sample	458	170	314
Calibration	170	458	314
Connecting	166	166	166
Separation	281	281	281

[a]Varying the potentials at the sample and calibration reservoirs does not affect the separation channel field strength as long as the sum of the voltages at the calibration and sample reservoirs remains constant.

Normally, when using the method of standard addition, a series of runs with varying known concentrations of analyte are added to a sample that contains the analyte in an unknown, yet constant concentration. The known added analyte concentration is then plotted against the total analyte signal. The absolute value of the x-intercept of a regression line through the data is the concentration of the analyte in the original sample. Performing the method of standard addition as explained above using the chip design shown in Fig. 2.1B would require that the analyte concentration in the calibration standard reservoir be changed by replacing the sample in the calibrant reservoir. This is not desirable for microchip devices that are to be used remotely or by relatively unskilled operators. Therefore, a slight modification to the standard addition method has been made. In this modification, the amount of analyte from the sample and calibrant reservoirs to the mixing channel is varied. The total analyte signal and the known amount of analyte from the calibration standard reservoir are then normalized to the percent contribution of analyte coming from the sample reservoir. This can be performed if the flow contribution (F) to the mixing channel from the calibration standard channel is known. The mixing ratio is determined by adding another compound to the calibration standard reservoir to serve as a flow indicator. The flow indicator signal for any run is normalized to its value at 100% flow, giving the fractional flows coming from both the calibration and sample reservoirs. The normalization constants for the total analyte signal and the calibration concentration standard are 1/(1 - F) and F/(1 - F), respectively. A plot then can be made of the normalized calibration standard concentration vs the normalized total analyte signal area. The absolute value of the x-intercept of a regression line through this data gives the concentration of the analyte in the original sample.

The sample in the analyte reservoir consisted of TRITC-Ala and TRITC-Asp. The analytes were introduced into the analyte reservoir at concentrations of 1, 3, 10, 30, and 100 µM. The analytes in the calibration reservoir were at a concentration of 10 µM. The percent flow from the analyte and calibration standard reservoirs into the mixing region was determined by adding TRITC-Arg to the calibration standard reservoir at a concentration of 10 µM. The flow from the calibration standard reservoir into the mixing region was varied in the following increments: 0, 0.25, 0.50, 0.75, and 1.00. The flow from the analyte reservoir into the mixing region was, therefore, the reverse of this. A typical standard addition curve obtained using the modified analysis method is shown in Fig. 2.5.

The results from all experiments performed are summarized in Table 2.3. The extrapolated concentrations for the 1-, 3-, and 10-µM samples are all within 0.6 µM of the actual concentration. The accuracy and precision of the results, however, need further improvement. The reason for the accuracy and precision problems deal with the experimental error added when extracting the normalized concentration information from the data. While the regression lines are all good at r = 0.999+, small errors in calculating the flow from each channel can introduce a large calculation error during the normalization process. The chip, however, can be redesigned to add another tee into the calibrant arm so that the method of standard additions could be implemented for analyte concentrations above the standard concentration. One of the channels feeding into this tee would continue to be the calibrant while the other channel would be a diluent. In this way the actual concentration of the calibrant could be programmatically changed by varying the potential at these two new reservoirs.

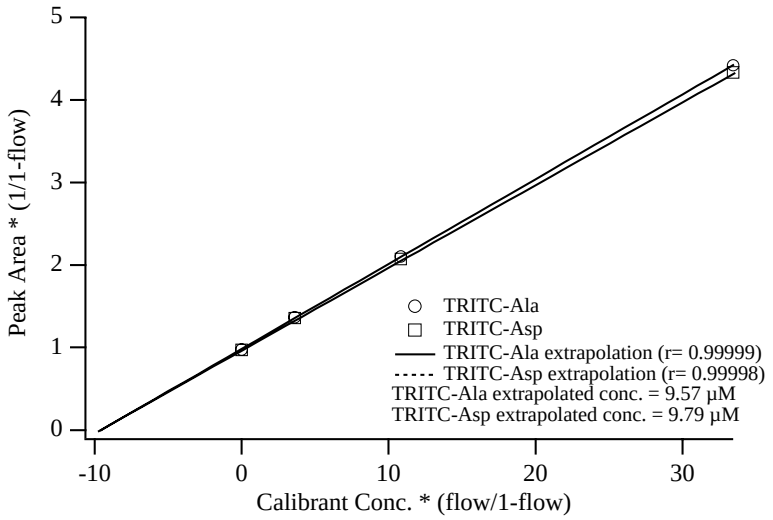

Fig. 2.5. Sample concentration determination using the modified method of standard additions.

Table 2.3. Extrapolated analyte concentrations using the modified standard addition method for microchip calibration.

Analytes	Sample concentration (µM)	Calculated concentration (µM)			
		Exp 1	Exp 2	Avg	Stdev
TRITC-Ala	1	0.98	2.08	1.53	0.78
	3	2.94	3.95	3.45	0.71
	10	8.95	9.87	9.46	0.47
TRITC-Asp	1	0.86	1.63	1.25	0.54
	3	3.00	3.91	3.46	0.64
	10	8.85	9.98	9.54	0.60

3. ENHANCED SEPARATIVE RESOLUTION

3.1 INTRODUCTION

As additional physical and chemical manipulations are integrated onto microchips, the complexity of fluid manipulation increases due to the number of channels and interconnections required for performing these steps. With this increase in complexity, improvements in valve control are central in maintaining or improving the efficiency of the process. Since many chip-based applications involve a separation, characterization of the injection process for the separation step could lead to overall improvement in chip performance. For the constant volume valve, the dimensions and concentration of the injected sample plug are controlled by two factors: the degree of spatial confinement within the cross intersection during sample loading and the electric field strength distribution during dispensing. The amount of spatial confinement at the intersection is controlled by adjusting the electric field strength in the sample channel (E_s) relative to the electric field strengths in the buffer (E_b) and analysis channels (E_a)(Fig. 3.1). To achieve symmetric sample confinement, E_b must equal E_a. As the ratio E_s/E_b decreases, the spatial confinement in the cross intersection increases. Varying the dispensing electric field strength ratios also controls the volume of sample injected. Increasing the electric field strengths in the sample (E_s) and sample waste (E_{sw}) channels relative to the analysis (E_a) channel reduces the amount of sample injected; decreasing these electric field strengths increases the amount of sample injected. This section of the report describes the effects of both the spatial confinement and the dispensing electric field distributions on the spatial extent and concentration of the injected sample plugs.

3.2 EXPERIMENTS

3.2.1 Microchip Design and Operation. The microchip channels on the substrate were fabricated using standard photolithographic techniques and chemical wet etching as explained in Section 2.2.1 above.[6] Figure 3.1 shows a schematic of the cross geometry used for the experiments. The enclosed column lengths from each reservoir to the injection cross were 7.9 mm for the buffer, 6.0 mm for the sample, 6.5 mm for the sample waste, and 26.4 mm for the analysis. The dimensions of the channels were measured with a surface profiler (P-10; Tencor Instruments) and were 10.2 μm deep, 56 μm wide at the top, and 48 μm wide at half depth.

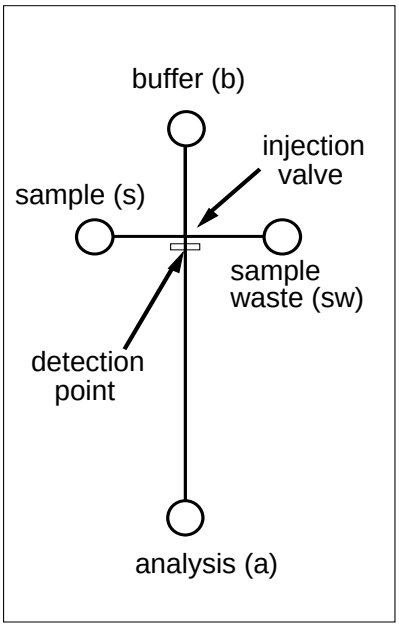

Fig. 3.1. Schematic diagram of cross microchip.

Rhodamine B (9.1 μM, Aldrich) was used as the test sample. The buffer used for all experiments was 10 mM sodium tetraborate (pH = 9.2, Aldrich).

The voltages were controlled using a single high-voltage power supply (10A12-P4; Ultravolt) with voltage division in 5% increments. The high voltage was toggled between the sample loading and sample dispensing steps using high-voltage relays (K81C245; Kilovac). The high-voltage power supply and relays were under computer control. Electrical contact between the high-voltage leads and reservoirs was made with platinum electrodes. The high-voltage control software and data acquisition software were written in-house using LabVIEW.

3.2.2 Single Point Detection. Temporal profiles were obtained using a single point detection system similar to that previously described.[15] Laser-induced fluorescence detection was performed using an argon ion laser (FRED 300; Coherent) operating at 514 nm with a power output of 7 mW. The laser beam was focused onto the analysis channel 100 μm from the injection cross. The fluorescence was collected through a 100X microscope objective (Mitutoyo) and focused onto a 200-μm-wide by 4-mm-long rectangular slit (Melles Griot). The fluorescence signal was then spectrally filtered using a 560-nm (Oriel) longpass filter before being measured by a photomultiplier tube (PMT; Oriel Instruments). The signal from the PMT was sent to a low-noise current preamplifier (SR570; Stanford Research System). The signal from the preamplifier was sampled at 1000 Hz using a multifunction I/O card (PCI-MIO-16XE50; National Instruments) in a G3 Power Macintosh.

3.2.3 Imaging. Two-dimensional images were obtained using a CCD (TE/CCD512TKM; Princeton Instruments) mounted on an inverted microscope (TE300; Nikon) equipped with a high-pressure mercury lamp.

3.3 RESULTS AND DISCUSSION

Three sample loading schemes were investigated with varying degrees of sample confinement in the cross intersection. For a homogeneous buffer and channel properties, the electric field strength in the sample waste channel, E_{sw}, is

$$E_{sw} = E_b + E_s + E_a$$

where E_x is the electric field strength in the sample waste (sw), buffer (b), sample (s) and analysis channel (a).

By adjusting E_s relative to E_b and E_a, the degree of sample confinement can be controlled. As the ratio E_s/E_b decreases, the spatial confinement in the cross intersection increases, resulting in a narrower sample stream. The electric field strengths in the buffer and analysis channel should be equal to provide a symmetrical pinch confinement profile. The three sample confinement levels investigated had E_s/E_b ratios of 9.0, 1.3, and 0.24. The "pinching effect" at these various ratios is qualitatively described as weak, medium, and strong, respectively. Figure 3.2b shows a fluorescence image of the strong pinch sample stream; Figs. 3.2c and d are images of the medium and weak pinched sample streams, respectively. The weak pinch sample dimensions were 108 μm at the valve entrance and 43 μm at the valve exit. The medium pinch focused the sample stream from 63 μm at the valve entrance to 24 μm at the exit, and the strong pinch

focused the sample stream from 29 μm to 10 μm (all measurements are full-width at half maximum).

Four dispensing schemes were investigated in conjunction with the three spatial confinement levels to provide additional control of the amount of sample injected into the analysis channel. Similar to the sample loading step, the electric field strength relationship for the dispensing step is $Eb = E_s + E_{sw} + E_a$. As E_s and E_{sw} are increased, the amount of sample dispensed into the analysis channel is reduced. Also, the electric field strengths in the sample and sample waste channels should be equal ($E_s = E_{sw}$) for symmetrical dispensing. In addition, the four dispensing steps here maintained nearly constant electric field strengths in the analysis channel so that any

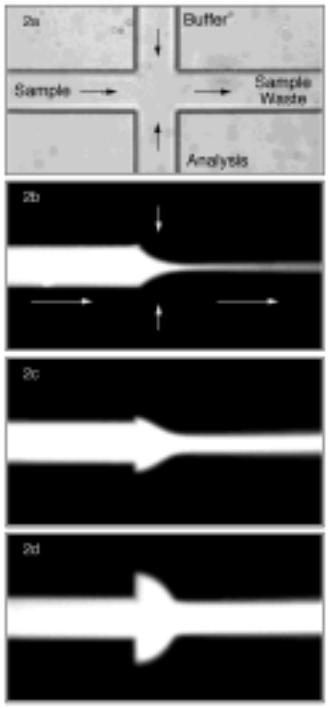

Fig. 3.2. CCD images of sample loading step: 2a: white light image, 2b: stong sample confinement, 2c: medium sample confinement, 2d: weak sample confinement.

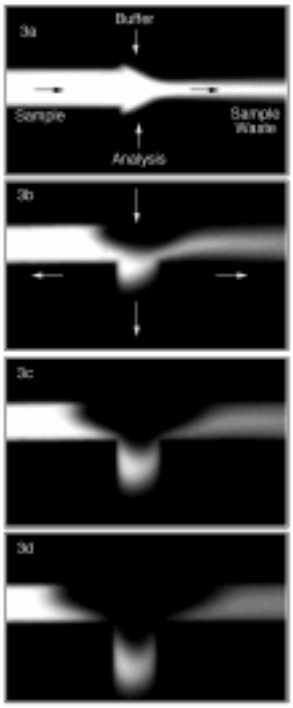

Fig. 3.3. CCD images of the sample plug formation process using the medium pinch and Case 2 dispensing scheme.

differences in efficiency are attributed to the dispensing step and not to other contributions such as diffusion. Table 3.1 summarizes the electric field strengths in the individual channels for the various sample confinement schemes and dispensing cases studied as well as relevant electric field strength ratios. Figure 3.3 shows a sequence of images depicting plug formation for the medium pinch and dispensing Case 2. Figure 3.3a shows the spatially confined sample during

Table 3.1. **Electric field strengths and ratios for the three sample loading and four dispensing modes.**

	E_b (kV/cm)	E_s (kV/cm)	E_{sw} (kV/cm)	E_a (kV/cm)	E_s/E_b	E_a/E_b
Weak Pinch	0.161	1.450	1.720	0.156	9.0	
Medium Pinch	0.441	0.581	1.309	0.333	1.3	
Strong Pinch	0.644	0.145	1.130	0.385	0.23	
Dispensing						
Case 1	1.576	0.654	0.604	0.292	0.415	0.19
Case 2	0.967	0.329	0.303	0.323	0.340	0.33
Case 3	0.737	0.200	0.185	0.343	0.271	0.47
Case 4	0.613	0.146	0.134	0.330	0.238	0.54

sample loading, subsequent dispensing steps (Fig. 3.3b, c), and the final injected plug (Fig. 3.3d).

The sample plug temporal profiles created by three different injection conditions are shown in Fig. 3.4a. These sample plugs were generated using the weak, medium, and strong pinch and dispensed using $E_a/E_b = 0.33$ (Case 2). As expected, the strong pinch shows the narrowest plug length compared to the medium and weak pinch. This also held true for the three other dispensing cases investigated.

Further control of the sample volume injected can be achieved by changing the electric field strengths in the sample and sample waste channels relative to the analysis channel during the dispensing step. As E_s and E_{sw} are increased, the amount of sample injected is decreased because a greater percentage of sample is drawn back into the sample and sample waste channels. Figure 3.4b shows representative peak profiles

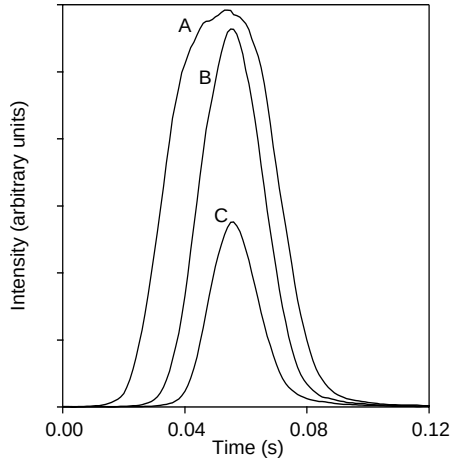

Fig. 3.4a. **Temporal profiles of different loading schemes (A: weak pinch, B: medium pinch, and C: strong pinch) with dispensing Case 2.**

of the four dispensing schemes with the identical sample confinement (medium pinch). The spatial extent of the profiles increases with the E_a/E_b ratio; Case 1 had the smallest peak and Case 4 injected the largest amount of sample.

Figure 3.5 shows the spatial variance of the four dispensing schemes for each of the three sample loading profiles. A comparison of the sample loading schemes dispensed under identical conditions (i.e., same dispensing case) shows the strong pinch gives the smallest spatial variance. The smallest reduction in the variance from weak to strong pinch was seen for dispensing Case 1 at 4.3 times. The improvements for dispensing Cases 2, 3, and 4 were 5.5, 6.0, and 6.3 times, respectively. The medium pinch produced spatial variances roughly three times smaller than the weak pinch.

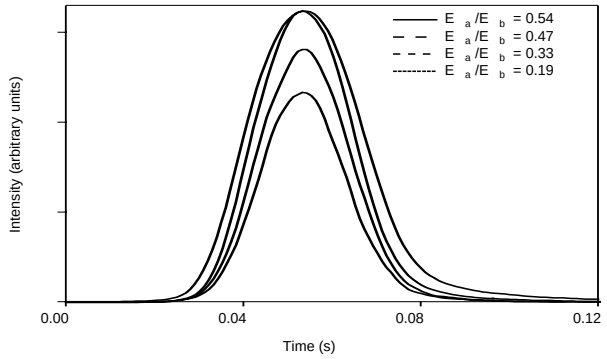

Fig. 3.4b. Temporal profiles of different dispensing schemes with the medium pinch sample loading.

Of the different dispensing schemes, Case 1 with the lowest E_a/E_b produced the smallest injected plug. Since E_a is held nearly constant for the four dispensing cases, the differences in the injected plug are attributed to the dispensing electric field strengths in the sample and sample waste channels. The spatial variances for the weak pinch for Cases 2, 3, and 4 are 1.3, 1.6, and 1.7 times that of Case 1, respectively; for the medium pinch, the variances for Cases 2, 3, and 4 are 1.2, 1.5, and 1.7 times that of Case 1. The different dispensing cases for the strong pinch had little effect on the sample plug variance. The change from Case 1 to Case 4 was only 1.1 times. The electric field strengths in the sample and sample waste channels have little effect on the sample plug variance for strongly pinched samples because of the tight confinement of the sample during the sample loading step. For the weak and medium pinch, the sample at the valve entrance is larger than the channel width (see Figs. 2c and d). For the strong pinch, the sample is confined within the channel (29-μm stream width vs 56-μm channel width). Therefore, the differences in

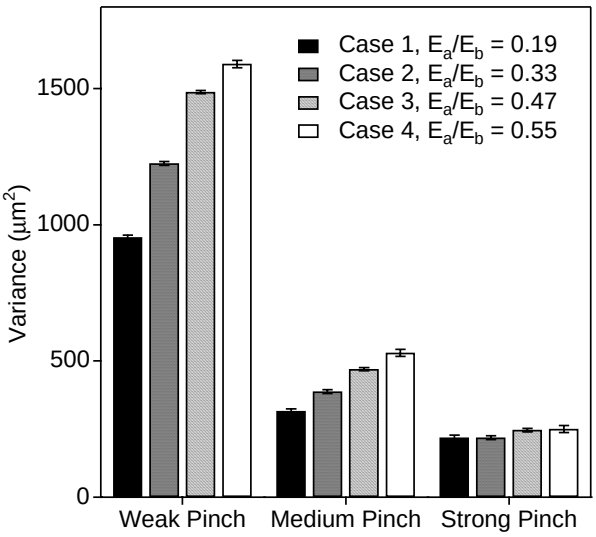

Fig. 3. 5. Spatial variance of dispensed plugs with pinch size and dispensing case (■ E_a/E_b = 0.19, ▒ E_a/E_b = 0.33, □ E_a/E_b = 0.47, □ E_a/E_b = 0.54).

the pull-back electric field strengths of the individual dispensing cases are not as pronounced. This helps explain the decrease in the variance when going from the weak pinch to the strong pinch.

The medium pinch was investigated further using different analysis channel electric field strengths. Figure 3.6 shows how the peak variance changes with migration time (analysis channel electric field strength) for the different dispensing cases. The total variance (σ^2_{tot}) is the sum of the variance due to the spatial extent of the detector (σ^2_{det}), diffusion (σ^2_{diff}), and injection plug length (σ^2_{inj}). The y-intercept of the fitted line is equal to $\sigma^2_{det} + \sigma^2_{inj}$. The variance due to the detector (σ^2_{det}) is 0.33 μm^2 and is negligible compared to the other sources of variance. For the four cases, σ^2_{inj} = 260 μm^2 (Case 1), 310 μm^2 (Case 2), 400 μm^2 (Case 3), and 440 μm^2 (Case 4). The slopes of the lines in Fig. 3.6 should equal two times the diffusion coefficient (D) of the sample. The diffusion coefficient for RhB in 10 mM borate was experimentally determined to be 4.2 x 10^{-6} cm^2 s^{-1}. One-half the average slope of the four lines in Fig. 3.6 is 4 x 10^{-6} cm^2 s^{-1} and is within experimental error with the previous measurement.

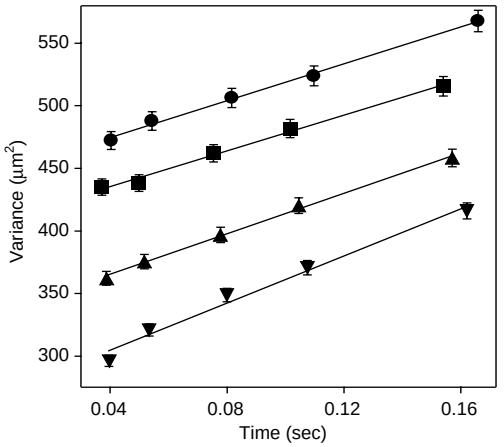

Fig. 3.6. Spatial variance of dispensed plugs for medium pinch vs migration time for the four dispensing cases (Case 1, Ea/Eb = .19; Case 2, Ea/Eb = .33; Case 3, Ea/Eb = .47; Case 4, Ea/Eb = .54).

Last, there is a trade-off between efficiency and detection sensitivity for the dispensed sample plugs. Smaller length sample plugs lead to higher separation efficiencies; however, this generally results in a loss of sensitivity. A balance, therefore, between sensitivity and efficiency was sought. The figure of merit used was a ratio of the peak height to the standard deviation of the peak width (h/σ). Figure 3.7 shows a plot of h/σ for the various sample confinement profiles versus E_a/E_b of the different dispensing cases. The sample plug that was loaded using the medium pinch provided the best ratio for each of the dispensing cases. Of the medium pinches, Case 3 (E_a/E_b = 0.47) displayed the highest h/σ ratio. The weak pinch profiles showed a steady decline from Case 1 to Case 4.

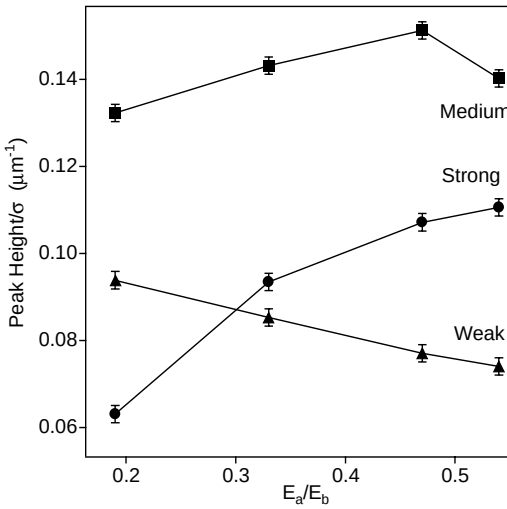

Fig. 3.7. Variation of the peak height/standard deviation (h/σ) ■ medium pinch, ▲ weak pinch, and ● strong pinch vs dispensing ratio (E_a/E_b).

This indicates the variance of the peaks (or injection plug width) increased at a faster rate than the signal increased. For the strong pinch, the opposite was true. There was an increase in h/σ as the electric field strengths in the sample and sample waste channels were decreased. Figure 3.5 showed that the variance of the strong pinch for the different dispensing ratios was nearly constant, indicating little effect on the plug width. The signal, however, increased by a factor of 2 from Case 1 to Case 4; therefore, the h/σ ratio increased by a factor of almost 2 (Fig. 3.5).

In conclusion, we have shown that the dispensed sample plug length can be controlled by both the sample loading and dispensing steps. The degree of sample confinement during the sample loading step played a larger role in determining the sample plug length than did the dispensing step. In fact, the more highly confined the sample is, the less of an effect the dispensing step had. As the sample is more highly pinched, the sample concentration in the cross intersection decreases at a much faster rate than the gain in sample plug variance. This increase in efficiency is offset by the decrease in sample dispensed. There is then a compromise between sensitivity and efficiency. This was evaluated using the peak height/peak standard deviation ratio.

4. DETECTION METHODS

4.1 INTRODUCTION

In this section we report a procedure to enhance the detection of analytes at low concentrations using sample stacking and sweeping.[25, 26] Hydrophobic test analytes were prepared in sample buffer (sodium tetraborate) and electrokinetically injected into a separation channel filled with run buffer (sodium tetraborate/SDS). The test analytes were swept and concentrated in the SDS micelle pesudostationary phase. In addition, the analytes in the swept zone also appeared to stack at the sample/run buffer interface. The combined effect of sweeping and stacking resulted in an 85- to 560-fold increase in concentration for the hydrophobic analytes in a 10-mm stacking distance. The concentration enhancement of the analytes obtained by the combined sweeping and stacking was greater than that achieved by sweeping alone.

4.2 EXPERIMENTS

4.2.1 Chemicals. A stock solution of buffer was made with sodium tetraborate (EM Science, Gibbstown, New Jersey) at a concentration of 100 mM and a pH of 9.3. The run buffer was made by dissolving SDS (Baker Inc., Phillipsburg, New Jersey) with the stock solution and water to yield a solution containing 100 mM SDS and 10 mM sodium tetraborate. The conductivity of the run buffer was determined by filling the microchip channels with the run buffer and measuring the current at a given field strength. The sample buffer was made by diluting the stock solution with water until it had the same conductivity as the run buffer. The sample buffer had a final concentration of 30 mM sodium tetraborate. Rhodamine 560 (R560), RhB, dichlorofluorescein (DCF) and rhodamine 6G (R6G) were purchased from Exciton, Inc. (Dayton, Ohio) and were used without further purification.

4.2.2 Microchip Device. The layout of the microchip is shown in Fig. 4.1. Reservoirs and channels are designated by the letters *a*-*d*, as shown, for reference in the text. The microchip was fabricated using standard photolithographic, wet chemical etching, and bonding techniques as previously described in Section 2.2.2. Channel dimensions were measured using a stylus-based surface profiler as reported in Section 3.2.1.

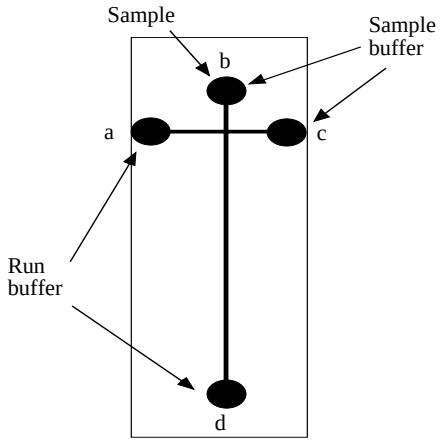

Fig. 4.1. Schematic of chip used for sample sweeping and stacking experiments.

4.2.3 Microchip Operation. The on-chip concentration process was recorded on videotape, and the images shown in this work were extracted from this videotape. In the single-point detection scheme, analyte fluorescence signals were monitored at specific points along channel *d* (see Fig. 4.1) with an Argon ion laser for excitation (488 nm and 10 mW for R560 and 514 nm and 10 mW for RhB, DCF, and R6G; Melles Griot, Irvine, California). The laser beam was focused to a spot in the channel with a 100-mm focal length lens (Newport, Irvine, California), and the fluorescence signal was collected using a 40X objective lens with a numerical aperture of 0.4. The signal was filtered spatially (1-mm-diam pinhole) and spectrally (540df40 bandpass filter; Omega Optical)). Computer programs written in LabVIEW were used for data acquisition and voltage control as described in Section 2.2.2. An in-house-built, high-voltage power supply with four individually controlled outputs was used to provide appropriate electric potentials at the microchip reservoirs via Pt electrodes as described in Section 2.2.2.

4.3 RESULTS AND DISCUSSION

The sweeping of the sample zones was carried out on a cross chip like the one shown in Fig. 4.1. Each reservoir was filled with buffer as labeled. The neutral hydrophobic dye RhB was dissolved in sample buffer in reservoir *b*. A gated valve scheme was employed to control buffer flow on the chip.[17] At each stage, the voltage at each reservoir was controlled such that the directions of the electroosmotic flow (EOF) are as indicated by the arrows in the image figures.

Sample buffer is constantly transported from channel *b* to channel *c*, and run buffer is transported from channel *a* to channel *c* at stage 1 (see Fig. 4.2A). There is some flow from channel *a* to *c*, which prevents the leaking of sample buffer from channel *b* into channel *d*. Since there is no RhB in reservoir *a*, channels *a* and *d* are not visible at this stage. The weak fluorescence signal in channel *b* is from unconcentrated RhB. When the RhB interacts with SDS micelles from channel *a* at the cross, it is "swept" and concentrated. This swept interface diffuses across the channel and results in a gradually widened and enhanced fluorescence signal in channel *c*.

During stage 2, the voltage applied at reservoirs *a* and *c* was floated for 2.5 s and the sample buffer from channel *b* was injected into channel *d* (see Fig. 4.2B). The intense fluorescence in

channel *d* was the result of the sweeping of hydrophobic RhB molecules by SDS micelles in run buffer. Although the voltage in reservoirs *a* and *c* was floated, there was still some leaking of run buffer from channel *a* into channel *d*, and this leaking run buffer also contributed to sample sweeping during the injection stage.

During stage 3, the voltage setting at reservoir *a* was switched back to that at stage 1 and the swept sample plug was trailed by run buffer. The swept sample plug (RhB/SDS micelle complex) was then stacked at the back of the sample plug (Fig. 4.2C). In Fig. 4.2D the entire sample plug has been swept and stacked at the back of the sample buffer interface, and the final zone size was about half that of the initial swept zone.

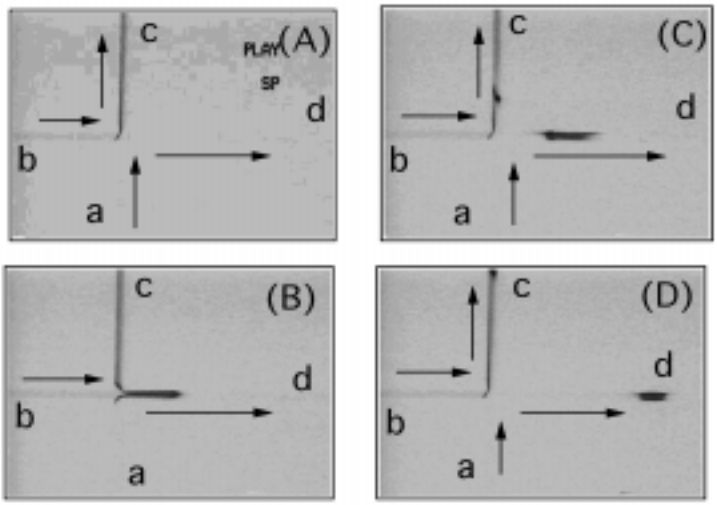

Fig. 4.2. Evolution of sweeping and stacking on a microchip using a gated valve. The sample buffer in reservoir b was doped with 24.4 μM of Rhodamine B. Arrows depict the direction of flow. (A) Stage 1 – voltage settings at each reservoir are *a*, 1.4; *b*, 1.5; *c*, 0.8; *d*, 0 kV. (B) Stage 2 (2.5-s injection) – voltage settings at each reservoir are *a*, 0.9; *b*, 1.5; *c*, 0.9; *d*, 0 kV. (C) 1 s into stage 3 – voltage settings are the same as those in stage 1. (D) 4 s into stage 3.

In the normal gated valve injection scheme described above, reservoirs *a* and *c* were floated during stage 2. Because it is difficult, however, to exactly match the potential applied to reservoirs *a* and *c* with that at the injection cross, run buffer will often leak into channel *d*. In order to make a sharper injection of the sample into the run buffer, therefore, the voltage applied to reservoirs *a* and *c* is lowered below that at the injection cross to create a net flow from reservoir *b* to reservoirs *a* and *c*. We call this modified gated injection a pull-back injection.

Stage 1 of the pull-back injection is similar to that of the normal gated injection scheme (Fig. 4.3A), except that no leakage from channel *d* occurs (Fig. 4.3B) because the sample plug has migrated slightly up the run buffer channel (channel *a*). The zone of intense fluorescence in channel *d* is the result of sweeping. A similar swept sample plug is also formed in channel *a* during the pull-back injection.

The electric field in channel *a* is switched back to that of stage 1 during stage 3, and the field in channel *a* is the reverse of that in stage 2. The back swept sample (BSS) is in a zone of lower electric field (higher net velocity), and the front swept sample (FSS) is in a zone of higher electric field (lower net velocity). Therefore, the BSS will catch up to the FSS. This is shown in Figs. 4.3C-F. The BSS develops a flat front after 0.12 s into stage 3 (Fig. 4.3C), which indicates the existence of a concentration boundary. At 1.3 s into stage 3, the BSS travels into channel *d*

(Fig. 4.3D), and the FSS had moves out of the current imaging frame to the right. The BSS moves closer to the FSS 3 s into stage 3 (Fig. 4E). At 7.5 s into stage 3, the BSS catches up with FSS. As shown in Fig. 4.3E, the FSS initially disperses but is later stacked into the BSS as shown in Fig. 4.3F. The final swept and stacked zone is only 300 µm in width, which is an 8-fold decrease in the zone size compared to that obtained in a single buffer system (30 mM sodium borate) under similar operating conditions.

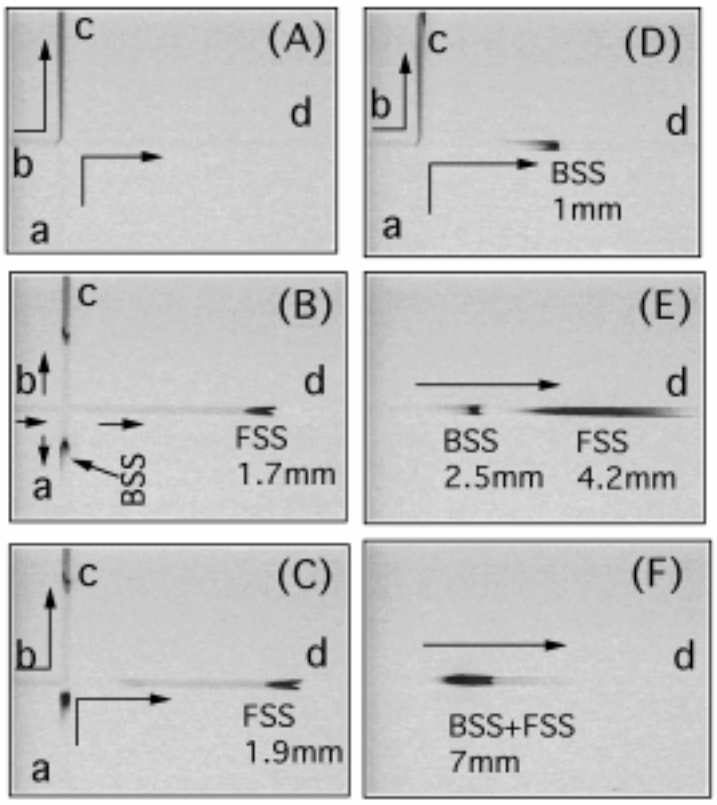

Fig. 4.3. Evolution of a stacked and swept sample zone. In stage 2 the voltage settings at each reservoir are *a*, 0.7; *b*, 1.5; *c*, 0.7; *d*, 0 kV. All other operating conditions are identical to that in Figure 4.2. The distance between swept sample and cross is as shown in each image: (A) stage 1; (B) stage 2 (3-s injection); (C) stage 3 (0.12 s into stage 3); (D) stage 3 (1.3 s into stage 3); (E) stage 4 (3 s); (F) stage 5 (7.5 s into stage 3)**.**

The effect of the injection time on the peak height, peak area, and peak width of the swept and stacked peaks was studied by monitoring sample plugs of RhB 10 mm from the cross in channel *d* with different injection times (see Fig. 4.4A). The maximum injection time under the operating conditions used in this experiment was 12 s, which allowed sweeping and stacking to be completed before the sample reached the detection point. The peak height and peak area increased approximately linearly with the injection time while the peak width decreased (see Fig. 4.4B). The RhB sample plugs with short injection times are swept and stacked closer to the injection cross and have a longer distance to travel to the detection point relative to peaks from longer injections. Since diffusion does not cause band dispersion until after sweeping and stacking is complete, the longer diffusion time for the short injections results in broader peaks.

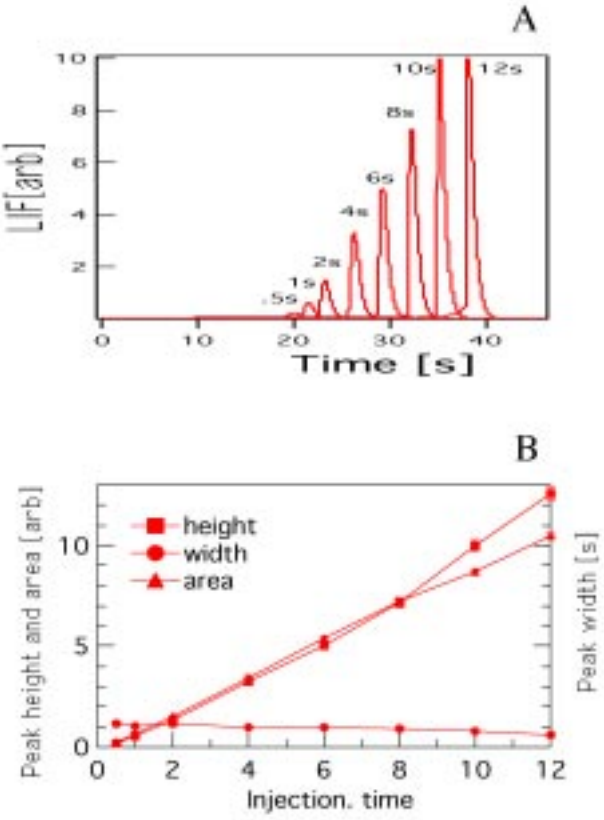

Fig. 4.4. The effects of injection time on peak height, area and width of stacked peak. Buffer location and chip operation are similar to that in Fig. 4.3. Sample buffer in reservoir *b* was doped with 2.44 μM of RhB. Detection was 10 mm from cross in channel *d*.

During the sample sweeping by SDS micelles in stage 2, the swept zone should be narrowed by a factor of 1/(1 + k), where k is the retention factor.[25, 26] The more hydrophobic the sample is, the narrower the swept zone will be. We found that the final zone length of swept samples after the stacking was correlated to the initial size of the swept zone and, therefore, to the hydrophobicity of the analyte. The signal enhancement factors of several test analytes are listed in Table 4.1. For a working distance of 10 mm, the peak height of swept and stacked R6G was 560 times greater than that obtained without stacking for an injection time of 25 s. Since the amount of injected sample is limited in these experiments only by the distance to the detection point, higher signal enhancements could be achieved using longer working distances for sweeping and stacking.

In conclusion, stacking of swept sample zone is an effective method for concentrating hydrophobic samples on microchips to enhance detection. Refinements in microchip design and operating conditions also are under investigation to further improve detection limits in chemical analyses.

Table 4.1. Enhancement factors of stacked and swept samples.

		R560	RhB	R6G
Factor of signal enhancement	8-s injection time	72	75	224
	Maximum injection time*	86 (10 s)	160 (15 s)	560 (25 s)

* Maximum injection time means that the front swept sample zone can not be stacked to the back swept sample zone before the detection at 10 mm from cross for injections longer than the maximum injection time.

5. REFERENCES

(1) Manz, A.; Harrison, D. J.; Verpoorte, E.; Widmer, H. M. In *Advances in Chromatography*; Brown, P. R., Grushka, E., Eds.; Marcel Dekker, Inc.: New York, 1993; Vol. 33, pp 1-66.

(2) Jacobson, S. C.; Ramsey, J. M. In *Handb. Capillary Electrophor. (2nd Ed.)*; Khaledi, M. G., Ed.; John Wiley & Sons, Inc.: New York, 1997; Vol. 146, pp 827-839.

(3) Harrison, D. J.; Fluri, K.; Seiler, K.; Fan, Z.; Effenhauser, C. S.; Manz, A. *Science*,**1993,** *261*, 895-897.

(4) Harrison, D. J.; Manz, A.; Fan, Z.; Luedi, H.; Widmer, H. M. *Anal. Chem.*,**1992,** *64*, 1926-1932.

(5) Effenhauser, C. S.; Manz, A.; Widmer, H. M. *Anal. Chem.*,**1993,** *65*, 2637-42.

(6) Jacobson, S. C.; Hergenröder, R.; Koutny, L. B.; Warmack, R. J.; Ramsey, J. M. *Anal. Chem.*,**1994,** *66*, 1107-1113.

(7) Jacobson, S. C.; Hergenröder, R.; Koutny, L. B.; Ramsey, J. M. *Anal. Chem.*,**1994,** *66*, 1114-1118.

(8) Effenhauser, C. S.; Paulus, A.; Manz, A.; Widmer, H. M. *Anal. Chem.*,**1994,** *66*, 2949-2953.

(9) Woolley, A. T.; Mathies, R. A. *Proc. Natl. Acad. Sci. U. S. A.*,**1994,** *91*, 11348-11352.

(10) Woolley, A. T.; Mathies, R. A. *Anal. Chem.*,**1995,** *67*, 3676-3680.

(11) von Heeren, F.; Verpoorte, E.; Manz, A.; Thormann, W. *Anal. Chem.*,**1996,** *68*, 2044-2053.

(12) Moore Jr., A. W.; Jacobson, S. C.; Ramsey, J. M. *Anal. Chem.*,**1995,** *67*, 4184-4189.

(13) Jacobson, S. C.; Hergenröder, R.; Koutny, L. B.; Ramsey, J. M. *Anal. Chem.*,**1994,** *66*, 2369-2373.

(14) Jacobson, S. C.; Hergenröder, R.; Moore, A. W., Jr.; Ramsey, J. M. *Anal. Chem.*,**1994,** *66*, 4127-4132.

(15) Jacobson, S. C.; Ramsey, J. M. *Anal. Chem.*,**1996,** *68*, 720-723.

(16) Chiem, N. H.; Harrison, D. J. *Clin. Chem.*,**1998,** *44*, 591-598.

(17) Jacobson, S. C.; Koutny, L. B.; Hergenröder, R.; Moore, A. W., Jr.; Ramsey, J. M. *Anal. Chem.*,**1994,** *66*, 3472-3476.

(18) Mangru, S. D.; Harrison, D. J. *Electrophoresis*,**1998,** *19*, 2301-2307.

(19) Hadd, A. G.; Raymond, D. E.; Halliwell, J. W.; Jacobson, S. C.; Ramsey, J. M. *Anal. Chem.*,**1997,** *69*, 3407-3412.

(20) Hadd, A. G.; Jacobson, S. C.; Ramsey, J. M. *Analytical Chemistry*,**1999,** *(ASAP article).*

(21) Waters, L. C.; Jacobson, S. C.; Kroutchinina, N.; Khandurina, J.; Foote, R. S.; Ramsey, J. M. *Anal. Chem.*,**1998,** *70*, 158-162.

(22) Waters, L. C.; Jacobson, S. C.; Kroutchinina, N.; Khandurina, J.; Foote, R. S.; Ramsey, J. M. *Anal. Chem.*,**1998,** *70*, 5172-5176.

(23) Kutter, J. P.; Jacobson, S. C.; Ramsey, J. M. *Anal. Chem.*,**1997,** *69*, 5165-5171.

(24) Kutter, J. P.; Jacobson, S. C.; Matsubara, N.; Ramsey, J. M. *Anal. Chem.*,**1998,** *70*, 3291-3297.

(25) Quirino, J. P.; Terabe, S. *Science*,**1998,** *282*, 465-468.

(26) Quirino, J. P.; Terabe, S. *Anal. Chem.*,**1999,** *71*, 1638-1644.

INTERNAL DISTRIBUTION

1–5. V. B. Baylor
6–9. J. M. Ramsey
10. Y-12 Central Files – RC

EXTERNAL DISTRIBUTION

11. Scott Smith, Central MASINT Office, 1030 South Hwy. A1A, Patrick Air Force Base, Florida 32925-3002